Towards Total Energy Shaping Control of Lower-Limb Exoskeletons

Ge Lv*, *Student Member, IEEE,* and Robert D. Gregg, *Senior Member, IEEE*

***Abstract*— Current robotic exoskeletons enforce fixed reference joint patterns during gait rehabilitation. These control methods aim to replicate normative joint kinematics but do not facilitate learning patient-specific kinematics. Trajectory-free control methods for exoskeletons are required to promote user control over joint kinematics. Our prior work on potential energy shaping provides virtual body-weight support through a trajectory-free control law, but altering only the gravitational forces does not assist the subject in accelerating/decelerating the body forward. Kinetic energy is velocity dependent and thus shaping the kinetic energy in addition to potential energy can yield greater dynamical changes in closed loop. In this paper, we generalize our previous work to achieve underactuated total energy shaping of the human body through a lower-limb exoskeleton. By shaping the fully-actuated part of the body's mass matrix, we satisfy the matching condition for different contact phases and obtain trajectory-free control laws. Simulations of a human-like biped demonstrate speed regulation in addition to body-weight support, indicating the potential clinical value of this control approach.**

I. INTRODUCTION

People suffering from stroke and other neurological diseases tend to walk slower, fall more frequently, and spend more metabolic energy while walking than able-bodied persons [1]. Different powered exoskeletons (or orthoses) have been developed to help these people regain mobility and confidence across different locomotor tasks. Vallery et al. [2] proposed an online reference trajectory generation method which generates reference kinematics in real time based on the unimpaired leg kinematics. The powered hip-knee exoskeleton ATLAS employs a finite-state machine controller to follow joint trajectories recorded from a healthy human subject [3]. The Hybrid Assistive Limb, designed for both augmenting healthy people's joint power and assisting people with gait disorders, tracks the pre-defined reference joint patterns based on the subject's intention during locomotion [4]. The control strategies of some other exoskeletons, such as the eLEGs and the Indego exoskeleton, also fall into the category of trajectory tracking [5], [6].

Although such systems could actively change joint behavior based on the user's behavior or environment, critical barriers in control technology still limit their adaptability. Kinematic control approaches aim to replicate normal joint kinematics associated with one specific task and user at a time [7], but fixed joint patterns may not facilitate learning during gait rehabilitation [8]. Patients should be allowed to adjust their kinematics during the learning process based on corrections from the therapist. Although some trajectory-free controllers have been proposed for amplifying human motion [9], [10] or compensating for exoskeleton mass/inertia [11], [12], these approaches assume that the user has the ability to fully produce the joint kinematics, which is not the case with weakened limbs. Exoskeletons require a novel control paradigm that promotes user control over joint kinematics.

Instead of tracking reference trajectories, kinetic goals (e.g., energy) could be enforced to provide a flexible learning environment during gait training. By controlling the human body's mechanical energy to either a constant level or an analytical function, exoskeletons could provide patients with some assistance while allowing them to control their own joint kinematics. Energy shaping has been applied to simple biped models to create natural, efficient gaits based on passive dynamics [13]. These approaches leverage the existence of unactuated "passive walking" gaits, which use only momentum and gravity to propel forward motion down a shallow slope [14]. The method of controlled symmetries shapes potential energy (rotating the gravity vector) to map passive gaits to actuated gaits on arbitrary slopes [15], [16]. Holm et al. achieved walking speed regulation through kinetic energy shaping in [17], [18], specifically scaling time or adding additional terms to the mass matrix.

Despite this rich body of work, practical limitations have prevented energy shaping from being adopted in human-like bipedal or wearable robots. Prior work has been limited to simple toy models where the matching conditions are tractable, especially the differential equation associated with kinetic energy shaping [19]. Similarly, these biped models have point feet or flat feet with a single contact model, often assuming full actuation. Humans are not point-footed or flat-footed walkers. In human walking, contact varies from heel to toe resulting in multiple periods of underactuation, which cannot be captured by the existing framework.

In our previous work, we considered the contact constraints encountered during human locomotion and applied underactuated potential energy shaping for orthosis control [20]. The trajectory-free shaping law generates virtual body-weight support (BWS) that alters the gravitational forces perceived by the human. However, shaping the potential energy alone does not help the patient accelerate/decelerate horizontally or achieve a desired walking speed. To further assist human locomotion, kinetic energy also needs to be shaped to render a greater change in the closed-loop dynam-

Asterisk indicates corresponding author.

G. Lv* is with the Departments of Electrical Engineering and Bioengineering, R. D. Gregg is with the Departments of Bioengineering and Mechanical Engineering, University of Texas at Dallas, Richardson, TX 75080, USA. {Ge.Lv, rgregg}@utdallas.edu

This work was supported by the National Institute of Child Health & Human Development of the NIH under Award Number DP2HD080349. The content is solely the responsibility of the authors and does not necessarily represent the official views of the NIH. R. D. Gregg holds a Career Award at the Scientific Interface from the Burroughs Wellcome Fund.

ics. By shaping the total mechanical energy of a system, we can augment human gaits in both the direction of walking and the direction of gravity. In this paper, we generalize the shaping framework proposed in [20]–[22] to achieve total energy shaping with contact constraints. We begin in Section II by modeling the biped and contact constraints for three phases of gait. Then, in Section III the generalized matching conditions for total energy shaping are satisfied to obtain control laws. Finally, we show potential benefits for gait rehabilitation with simulations of an 8-degree of freedom (DoF) biped in Section IV.

II. Modeling and Dynamics

For this case study, we are interested in controlling a bilateral powered hip-knee-ankle exoskeleton, where the biped model is shown in Fig. 1. Because this model is planar we combine two hip joints into one. We also assume masses m_i, $i \in \{\mathrm{f}, \mathrm{s}, \mathrm{t}, \mathrm{h}\}$, shown in Fig. 1 are the combined masses of the human limb and the exoskeleton.

A. Combined Human and Exoskeleton Model

The exoskeleton is modeled as a kinematic chain with respect to an inertial reference frame (IRF) defined at either the stance heel or stance toe, depending on the phase of the single-support period (Fig. 2). The configuration is given by $q = (p_{\mathrm{x}}, p_{\mathrm{y}}, \phi, \theta_{\mathrm{a}}, \theta_{\mathrm{k}}, \theta_{\mathrm{h}}, \theta_{\mathrm{sk}}, \theta_{\mathrm{sa}})^T \in \mathbb{R}^{8\times 1}$, where p_{x} and p_{y} are the Cartesian coordinates of the heel, ϕ is the angle of the heel defined with respect to the vertical axis, θ_{a} and θ_{k} are the angles of the stance ankle and stance knee, θ_{h} is the hip angle defined between the stance and swing thighs, and θ_{sk} and θ_{sa} are the angles of the swing knee and swing ankle, respectively. The Lagrangian dynamics can be derived in the form

$$M(q)\ddot{q} + C(q,\dot{q})\dot{q} + N(q) + A(q)^T\lambda = \tau, \tag{1}$$

where $M(q)$ is the inertia/mass matrix, $C(q,\dot{q})$ is the Coriolis/centrifugal matrix, and $N(q)$ is the gravitational forces vector. The constraint matrix $A(q) \in \mathbb{R}^{c\times 8}$ is defined as the gradient of the constraint functions, where c is the number of contact constraints that may change during different contact conditions. The Lagrange multiplier λ represents the ground reaction forces and is calculated using the method in [23]. Assuming both the exoskeleton and human have actuation at the ankle, knee, and hip joints, the overall torque input τ on the right-hand side of (1) comprises actuator torques $\mathrm{u} = [u_{\mathrm{a}}, u_{\mathrm{k}}, u_{\mathrm{h}}, u_{\mathrm{sk}}, u_{\mathrm{sa}}]^T \in \mathbb{R}^{5\times 1}$ and human muscular input $\mathrm{v} = [v_{\mathrm{a}}, v_{\mathrm{k}}, v_{\mathrm{h}}, v_{\mathrm{sk}}, v_{\mathrm{sa}}]^T \in \mathbb{R}^{5\times 1}$, where the subscripts indicate the ankle, knee, hip, swing knee, and swing ankle, respectively. Both u and v are mapped into the coordinate system by $B = (0_{5\times 3}, I_{5\times 5})^T \in \mathbb{R}^{8\times 5}$, i.e., $\tau = B\mathrm{u} + B\mathrm{v}$.

B. Holonomic Contact Constraints

The single-support period of human walking can be separated into heel contact, flat foot, and toe contact phases, based on which appropriate holonomic contact constraints can be defined as in Fig. 2. The holonomic contact constraints of our biped model can be expressed as relations between the position variables of the form

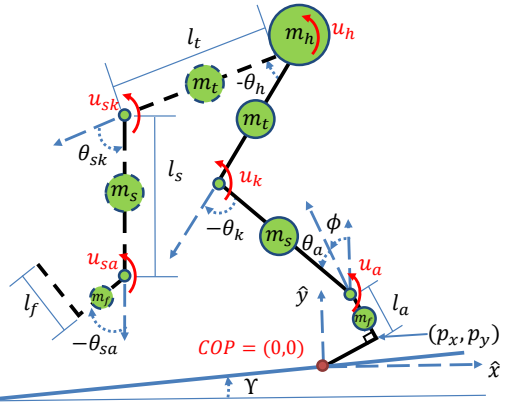

Fig. 1. Kinematic model of the biped, where the stance leg is shown in solid black and the swing leg in dashed black. For simulation study, we assume the biped is walking on a slope with angle γ. The red arcs indicate the joints that are actuated by both the exoskeleton and human, and COP denotes the Center of Pressure.

$$a(q_1, q_2, ..., q_c) = 0_{c\times 1}, \tag{2}$$

where q_j denotes the j-th element of the configuration vector q. There are $c = 2$ constraints for heel contact and toe contact whereas flat foot has $c = 3$. In this paper we assume the constraint matrix A has the following constant form:

$$A = \nabla_q a(q) = [I_{c\times c} \quad 0_{c\times(n-c)}], \tag{3}$$

where $n = 8$ is the number of DoFs. This form can be achieved by defining the IRF at the stance heel during heel contact and flat foot vs. the stance toe during toe contact.

III. Energy Shaping with Contact Constraints

In this section we will first review the definition of traditional energy shaping, and then we will incorporate holonomic contact constraints to define the so-called *equivalent constrained dynamics*, and matching conditions for kinetic energy, potential energy and human input, respectively. Finally we prove the matching conditions are satisfied for a class of shaped Lagrangians.

A. Energy Shaping Control

Consider a forced Euler-Lagrange system with configuration space $\mathbb{Q}$, taken for simplicity to be equal to $\mathbb{R}^n$, and described by a Lagrangian $L : T\mathbb{Q} \to \mathbb{R}$:

$$L(q,\dot{q}) = \frac{1}{2}\dot{q}^T M(q)\dot{q} - P(q), \tag{4}$$

where $\frac{1}{2}\dot{q}^T M(q)\dot{q}$ is the kinetic energy and $P(q)$ is the potential energy. The Lagrangian dynamics are given by

$$\frac{d}{dt}\partial_{\dot{q}} L(q,\dot{q}) - \partial_q L(q,\dot{q}) = B(q)\tau, \tag{5}$$

where $B(q) : \mathbb{R}^p \to T_q{}^*\mathbb{Q} \simeq \mathbb{R}^n$ with rank p maps the torque vector $\tau \in \mathbb{R}^p$ into the dynamical system, and $p < n$ indicates the system is underactuated. We can express (5) in the following form for a mechanical system:

$$M(q)\ddot{q} + C(q,\dot{q})\dot{q} + N(q) = B(q)\tau, \tag{6}$$

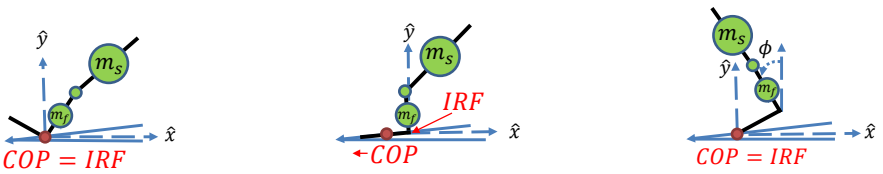

Fig. 2. Heel contact condition (left), flat foot condition (center), and toe contact condition (right) during single-support period on a slope with angle γ. The position of the heel is given by (p_x, p_y) and the position of the toe is given by $(\bar{p}_x, \bar{p}_y)$.

where terms on the left-hand side are defined similarly to (1) with $N(q) = \nabla_q P(q)$.

Now consider an unforced Euler-Lagrange system defined by another Lagrangian $\tilde{L} : T\mathbb{Q} \to \mathbb{R}$:

$$\tilde{L}(q, \dot{q}) = \frac{1}{2}\dot{q}^T \tilde{M}(q)\dot{q} - \tilde{P}(q) \tag{7}$$

for a new kinetic energy $\frac{1}{2}\dot{q}^T\tilde{M}(q)\dot{q}$ and new potential energy $\tilde{P}(q)$, resulting in the dynamics

$$\begin{aligned} \frac{d}{dt}\partial_{\dot{q}}\tilde{L}(q,\dot{q}) - \partial_q \tilde{L}(q,\dot{q}) &= 0 & (8)\\ \Leftrightarrow\ \tilde{M}(q)\ddot{q} + \tilde{C}(q,\dot{q})\dot{q} + \tilde{N}(q) &= 0 & (9) \end{aligned}$$

with $\tilde{N}(q) = \nabla_q \tilde{P}(q)$ being the desired gravitational forces.

These two systems are said to match if there exists a control law that brings system (6) into (9). Subtracting (9) from (6) and omitting q and $\dot{q}$ in the dynamical terms to abbreviate notations, we obtain

$$B\tau = M\ddot{q} + C\dot{q} + N - (\tilde{M}\ddot{q} + \tilde{C}\dot{q} + \tilde{N}). \tag{10}$$

Solving for $\ddot{q}$ from (9) and plugging this into (10), we have

$$B\tau = C\dot{q} + N - M\tilde{M}^{-1}(\tilde{C}\dot{q} + \tilde{N}). \tag{11}$$

Standard results in [24] shows that systems (6) and (9) match if and only if there exists a full-rank left annihilator $B(q)^\perp \in \mathbb{R}^{(n-p)\times n}$ of $B(q)$, i.e., $B(q)^\perp B(q) = 0$ and $\mathrm{rank}(B(q)^\perp) = n - p$, $\forall q \in \mathbb{Q}$, such that

$$B^\perp[C\dot{q} + N - M\tilde{M}^{-1}(\tilde{C}\dot{q} + \tilde{N})] = 0. \tag{12}$$

Equation (12) is the so-called *Matching Condition*. Assuming (12) is satisfied, the control law that achieves the closed-loop dynamics (9) is given as

$$\tau = (B^T B)^{-1} B^T [C\dot{q} + N - M\tilde{M}^{-1}(\tilde{C}\dot{q} + \tilde{N})]. \tag{13}$$

B. Equivalent Constrained Dynamics

In this part, we will plug expressions for A and λ into (1) in order to obtain the equivalent constrained dynamics in the form of (6). The Lagrangian multiplier λ is calculated based on the results in [23] as

$$\begin{aligned} &\lambda = \hat{\lambda} + \tilde{\lambda}\mathrm{u},\\ &\hat{\lambda} = W(\cancel{\dot{A}\dot{q}} - AM^{-1}(C\dot{q} + N - B\mathrm{v})),\\ &\tilde{\lambda} = WAM^{-1}B, \quad \text{where} \quad W = (AM^{-1}A^T)^{-1}. \end{aligned}$$

Plugging in λ, dynamics (1) become:

$$M_\lambda\ddot{q} + C_\lambda\dot{q} + N_\lambda = B_\lambda \mathrm{u} + B_\lambda \mathrm{v}, \tag{14}$$

where
$$\begin{aligned} M_\lambda &= M,\\ C_\lambda &= (I - A^T WAM^{-1})C + \cancel{A^T W\dot{A}},\\ B_\lambda &= (I - A^T WAM^{-1})B,\\ N_\lambda &= (I - A^T WAM^{-1})N. \end{aligned} \tag{15}$$

For total energy shaping, we define our closed-loop equivalent constrained dynamics in the form of (9) given the open-loop dynamics (14):

$$\tilde{M}_\lambda\ddot{q} + \tilde{C}_\lambda\dot{q} + \tilde{N}_\lambda = \tilde{B}_\lambda \mathrm{v}, \tag{16}$$

where v is the human input in the closed-loop dynamics. The other dynamics terms are defined as:

$$\begin{aligned} &\tilde{M}_\lambda = \tilde{M},\\ &\tilde{C}_\lambda = (I - A^T\tilde{W}A\tilde{M}^{-1})\tilde{C} + \cancel{A^T\tilde{W}\dot{A}},\\ &\tilde{B}_\lambda = (I - A^T\tilde{W}A\tilde{M}^{-1})\tilde{B},\\ &\tilde{N}_\lambda = (I - A^T\tilde{W}A\tilde{M}^{-1})\tilde{N},\\ &\tilde{W} = (A\tilde{M}^{-1}A^T)^{-1}. \end{aligned} \tag{17}$$

Given (17), we follow the procedure from (6) to (12) to derive the matching condition for the equivalent constrained dynamics, which is given as:

$$\begin{aligned} B_\lambda^\perp[M_\lambda\tilde{M}_\lambda^{-1}(\tilde{B}_\lambda\mathrm{v} - \tilde{C}_\lambda\dot{q} - \tilde{N}_\lambda)\\ + C_\lambda\dot{q} + N_\lambda - B_\lambda\mathrm{v}] = 0. \end{aligned} \tag{18}$$

We can separate (18) into three sub-conditions:

$$B_\lambda^\perp(C_\lambda\dot{q} - M_\lambda\tilde{M}_\lambda^{-1}\tilde{C}_\lambda\dot{q}) = 0, \tag{19}$$
$$B_\lambda^\perp(N_\lambda - M_\lambda\tilde{M}_\lambda^{-1}\tilde{N}_\lambda) = 0, \tag{20}$$
$$B_\lambda^\perp(B_\lambda\mathrm{v} - M_\lambda\tilde{M}_\lambda^{-1}\tilde{B}_\lambda\mathrm{v}) = 0, \tag{21}$$

where these three sub-conditions correspond to the matching for kinetic energy, potential energy, and human muscular input, respectively. The control law that brings (14) into (16) is given as:

$$\begin{aligned} \mathrm{u} = (B_\lambda^T B_\lambda)^{-1}B_\lambda^T[M_\lambda\tilde{M}_\lambda^{-1}(\tilde{B}_\lambda\mathrm{v} - \tilde{C}_\lambda\dot{q} - \tilde{N}_\lambda)\\ + C_\lambda\dot{q} + N_\lambda - B_\lambda\mathrm{v}]. \end{aligned} \tag{22}$$

Note that the control law u depends on M_λ and $\tilde{M}_\lambda$, which include anatomical parameters such as human limb ineritas/masses. Although these parameters are difficult to measure in practice and estimation errors may exist, it may be possible to establish a passivity property similar to [21] in order to guarantee safe human-machine interaction, i.e., an inaccurate control law will not harm the user.

Because the human input term v is not easily measured in practice, we choose the closed-loop mapping $\tilde{B}_\lambda$ such that v disappears from the exoskeleton control law (22):

$$\tilde{B}_\lambda = \tilde{M}_\lambda M_\lambda^{-1} B_\lambda, \tag{23}$$

which solves the equality $B_\lambda \mathrm{v} - M_\lambda \tilde{M}_\lambda^{-1} \tilde{B}_\lambda \mathrm{v} = 0$. This choice alters the way that human input v enters the closed-loop system dynamics and immediately satisfies the matching condition (21). Hence, only the matching conditions (19) and (20) will need to be satisfied in the following section.

C. Matching Proof with Contact Constraints

Prior research showed that the bottom-right submatrix of a mass matrix is the mass matrix of a lower-dimensional mechanical system [13]. This motivates us to shape the bottom-right part in M, which may render matching conditions that are easier to satisfy. In this paper we only consider the constant case for matrix A in (3); generalizing to the case of $\dot{A}(q) \neq 0$ is left to future work.

To begin the matching proof, we decompose M in the same manner shown in [20], [21]:

$$M = \begin{bmatrix} M_1 & M_2 \\ M_2^T & M_4 \end{bmatrix} = M_\lambda \tag{24}$$

where $M_1 \in \mathbb{R}^{c\times c}$, $M_2 \in \mathbb{R}^{c\times(n-c)}$, and $M_4 \in \mathbb{R}^{(n-c)\times(n-c)}$. We will shape the right-bottom term, i.e.,

$$\tilde{M} = \begin{bmatrix} M_1 & M_2 \\ M_3 & \tilde{M}_4 \end{bmatrix} = \tilde{M}_\lambda, \tag{25}$$

where the choice of $\tilde{M}_4$ will be specified later. We will now satisfy the matching conditions for this case.

1) Kinetic Energy: Note from [17], [18] that we have the relationship between C and M as follows:

$$C\dot{q} = D_q(M\dot{q})\dot{q} - \frac{1}{2}\partial_q(\dot{q}^T M \dot{q}), \tag{26}$$

where $D_x(y)$ is the Jacobian matrix of partial derivatives of vector y with respect to vector x. Because the first c DoFs are constrained, their time-derivatives equal zero in (26):

$$C\dot{q} = D_q \begin{bmatrix} M_2\dot{q}_{c+1,n} \\ M_4\dot{q}_{c+1,n} \end{bmatrix} \cdot \begin{bmatrix} 0 \\ \dot{q}_{c+1,n} \end{bmatrix} - \frac{1}{2}\partial_q(\dot{q}_{c+1,n}^T M_4 \dot{q}_{c+1,n}),$$

Moreover, submatrix M_4 does not depend on $q_{1,c}$ based on the recursively cyclic property in [13], yielding simplified expressions for $C\dot{q}$ and $\tilde{C}\dot{q}$:

$$C\dot{q} = \begin{bmatrix} \partial_{q_{c+1,n}}(M_2\dot{q}_{c+1,n})\dot{q}_{c+1,n} \\ \Psi \end{bmatrix}, \tag{27}$$

$$\tilde{C}\dot{q} = \begin{bmatrix} \partial_{q_{c+1,n}}(M_2\dot{q}_{c+1,n})\dot{q}_{c+1,n} \\ \tilde{\Psi} \end{bmatrix}, \tag{28}$$

where

$$\Psi := \frac{1}{2}\partial_{q_{c+1,n}}(\dot{q}_{c+1,n}^T M_4 \dot{q}_{c+1,n}) \in \mathbb{R}^{(n-c)\times 1},$$
$$\tilde{\Psi} := \frac{1}{2}\partial_{q_{c+1,n}}(\dot{q}_{c+1,n}^T \tilde{M}_4 \dot{q}_{c+1,n}) \in \mathbb{R}^{(n-c)\times 1}.$$

Following the same procedure in [21], we calculate $[I - A^T W A M^{-1}]$ in (14) using the *Blockwise Inversion* of M and define $[I - A^T \tilde{W} A \tilde{M}^{-1}]$ accordingly:

$$[I - A^T W A M^{-1}] = \begin{bmatrix} 0_{c\times c} & Y \\ 0_{(n-c)\times c} & I_{(n-c)\times(n-c)} \end{bmatrix}, \tag{29}$$

$$[I - A^T \tilde{W} A \tilde{M}^{-1}] = \begin{bmatrix} 0_{c\times c} & \tilde{Y} \\ 0_{(n-c)\times c} & I_{(n-c)\times(n-c)} \end{bmatrix}, \tag{30}$$

where $Y = M_2 M_4^{-1}$, and $\tilde{Y} = M_2 \tilde{M}_4^{-1}$. Multiplying (29) with (27) and (30) with (28), we obtain

$$C_\lambda \dot{q} = \begin{bmatrix} Y\Psi \\ \Psi \end{bmatrix}, \ \tilde{C}_\lambda \dot{q} = \begin{bmatrix} \tilde{Y}\tilde{\Psi} \\ \tilde{\Psi} \end{bmatrix}. \tag{31}$$

The blockwise inversion method is used again to simplify the multiplication between M_λ and $\tilde{M}_\lambda^{-1}$ in (18):

$$M_\lambda \tilde{M}_\lambda^{-1} = \begin{bmatrix} I_{c\times c} & 0_{c\times(n-c)} \\ \Omega_1 & \Omega_2 \end{bmatrix}, \tag{32}$$

where $\Omega_1 = (I - M_4\tilde{M}_4^{-1})M_3(M_1 - M_2\tilde{M}_4^{-1}M_3)^{-1} \in \mathbb{R}^{(n-c)\times c}$ and $\Omega_2 = -\Omega_1\tilde{Y} + M_4\tilde{M}_4^{-1} \in \mathbb{R}^{(n-c)\times(n-c)}$. The matrix B_λ is calculated from (15) and its annihilator $B_\lambda^\perp$ is chosen as follows:

$$B_\lambda = \begin{bmatrix} YB_{(c+1,n)} \\ B_{(c+1,n)} \end{bmatrix}, \ B_\lambda^\perp = \begin{bmatrix} I_{c\times c} & -Y \\ 0_{(n-p-c)\times c} & S \end{bmatrix}, \tag{33}$$

where $S = [I_{(n-p-c)\times(n-p-c)}, \ 0_{(n-p-c)\times p}]$, and the subscript (i,k) indicates rows i through k of a matrix. When the system is fully-actuated, i.e., $n = p + c$, the second row of the annihilator disappears. It can be verified that $B_\lambda^\perp \in \mathbb{R}^{(n-p)\times n}$, $\mathrm{rank}(B_\lambda^\perp) = n - p$, and $B_\lambda^\perp B_\lambda = 0_{(n-p)\times p}$. Plugging $B_\lambda^\perp$, (32), and (31) into (19), the left-hand side of the matching condition becomes

$$\begin{aligned} &B_\lambda^\perp[C_\lambda\dot{q} - M_\lambda\tilde{M}_\lambda^{-1}\tilde{C}_\lambda\dot{q}] \\ &= \begin{bmatrix} I_{c\times c} & -Y \\ 0_{(n-p-c)\times c} & S \end{bmatrix} \begin{bmatrix} Y\Psi - \tilde{Y}\tilde{\Psi} \\ \Psi - \Omega_1\tilde{Y}\tilde{\Psi} - \Omega_2\tilde{\Psi} \end{bmatrix}. \end{aligned} \tag{34}$$

The first c rows of (34) simplify as follows:

$$\begin{aligned} &[I_{c\times c} \quad -Y] \begin{bmatrix} Y\Psi - \tilde{Y}\tilde{\Psi} \\ \Psi - \Omega_1\tilde{Y}\tilde{\Psi} - \Omega_2\tilde{\Psi} \end{bmatrix} \\ &= (-\tilde{Y} + Y\Omega_1\tilde{Y} + Y\Omega_2)\tilde{\Psi} = (-\tilde{Y} + YM_4\tilde{M}_4^{-1})\tilde{\Psi} \\ &= (-\tilde{Y} + M_2\tilde{M}_4^{-1})\tilde{\Psi} = 0_{c\times 1}. \end{aligned} \tag{35}$$

For our case, $n = 8$, $p = 5$, and c equals to 2 or 3 based on the contact condition. During flat foot the system is fully actuated, hence the second row of $B_\lambda^\perp$ vanishes and (19) is satisfied through (35). However, heel or toe contact results in underactuation ($n > p + c$) and thus additional analysis is needed to fully satisfy the matching condition (19).

Note that during underactuated cases, M_4 cannot be shaped arbitrarily. We propose satisfying the matching condition by shaping only the bottom-right $p\times p$ part of M_4, which is associated with the p actuated coordinates. To show this, we first decompose M_4 and shape M_4 in a similar manner to (25):

$$M_4 = \begin{bmatrix} M_{41} & M_{42} \\ M_{42}^T & M_{44} \end{bmatrix}, \ \tilde{M}_4 = \begin{bmatrix} M_{41} & M_{42} \\ M_{42}^T & \tilde{M}_{44} \end{bmatrix},$$

where $M_{41} \in \mathbb{R}^{(n-p-c)\times(n-p-c)}$, $M_{42} \in \mathbb{R}^{(n-p-c)\times p}$, and $M_{44}, \tilde{M}_{44} \in \mathbb{R}^{p\times p}$. Similar to (32), the top-left element of $M_4\tilde{M}_4^{-1}$ will be $I_{(n-p-c)\times(n-p-c)}$. Subtracting $M_4\tilde{M}_4^{-1}$ from $I_{(n-c)\times(n-c)}$, the first $(n-p-c)$ rows of Ω_1 will become zeroes. As a consequence, the first $(n-p-c)$ rows of Ω_2 become $[I_{(n-p-c)\times(n-p-c)},\ 0_{(n-p-c)\times p}]$. Leveraging these properties of Ω_1 and Ω_2, the bottom $(n-p-c)$ rows of (34) become

$$\begin{aligned}&\begin{bmatrix}0_{(n-p-c)\times c} & S\end{bmatrix}\begin{bmatrix}Y\Psi - \tilde{Y}\tilde{\Psi}\\ \Psi - \Omega_1\tilde{Y}\tilde{\Psi} - \Omega_2\tilde{\Psi}\end{bmatrix}\\ &= \frac{1}{2}\partial_{q(c+1,n-p)}(\dot{q}_{c+1,n}^T(M_4 - \tilde{M}_4)\dot{q}_{c+1,n}). \end{aligned} \tag{36}$$

From [13], we know $q_{(c+1,n-p)}$ is cyclic in $M_{44} \in \mathbb{R}^{p\times p}$, i.e., $\partial M_{44}/\partial q_{(c+1,n-p)} = 0$, hence (36) equals $0_{(n-p-c)\times 1}$ and the matching condition (19) is satisfied.

2) Potential Energy: The constrained potential forces vectors are obtained from (15) and (17) as

$$N_\lambda = \begin{bmatrix}YN_{c+1,n}\\ N_{c+1,n}\end{bmatrix},\ \ \tilde{N}_\lambda = \begin{bmatrix}\tilde{Y}\tilde{N}_{c+1,n}\\ \tilde{N}_{c+1,n}\end{bmatrix}. \tag{37}$$

Similar to the matching proof for *Kinetic Energy*, plugging $B_\lambda^\perp$, (32), and (37) into (20), the first c rows of the matching condition become:

$$\begin{aligned}&\begin{bmatrix}I_{c\times c} & -Y\end{bmatrix}[N_\lambda - M_\lambda\tilde{M}_\lambda^{-1}\tilde{N}_\lambda]\\ &= \begin{bmatrix}I_{c\times c} & -Y\end{bmatrix}\begin{bmatrix}YN_{c+1,n} - \tilde{Y}\tilde{N}_{c+1,n}\\ N_{c+1,n} - \Omega_1\tilde{Y}\tilde{N}_{c+1,n} - \Omega_2\tilde{N}_{c+1,n}\end{bmatrix}\\ &= (-\tilde{Y} + Y\Omega_1\tilde{Y} + Y\Omega_2)\tilde{N}_{(c+1,n)} = 0_{c\times 1}, \end{aligned} \tag{38}$$

which can be verified based on (35). Again, (38) serves as the matching condition (20) for the fully-actuated conditions. For underactuated cases, we need to check the additional $(n-p-c)$ rows of the matching condition:

$$\begin{aligned}&\begin{bmatrix}0_{(n-p-c)\times c} & S\end{bmatrix}[N_\lambda - M_\lambda\tilde{M}_\lambda^{-1}\tilde{N}_\lambda]\\ &= S\cdot(N_{c+1,n} - \Omega_1\tilde{Y}\tilde{N}_{c+1,n} - \Omega_2\tilde{N}_{c+1,n})\\ &= N_{(c+1,n-p)} - \tilde{N}_{(c+1,n-p)}, \end{aligned} \tag{39}$$

where we again leverage the above mentioned properties of Ω_1 and Ω_2. As in [20] this matching condition can be satisfied by assuming $N_{(c+1,n-p)} = \tilde{N}_{(c+1,n-p)}$. We will make the same assumption here to satisfy the matching condition (20).

IV. Simulation Results

Now that we have designed controller (22) and proved that it will shape total energy, we wish to study it during simulated walking with the biped model. To start, we first specify our choice of $\tilde{M}_{44}$ and $\tilde{N}_\lambda$. Note that for fully-actuated cases shaping M_{44} coincides with shaping M_4.

A. Choice of $\tilde{M}_{44}$ and $\tilde{N}_\lambda$: A Case Study

Prior work [11] indicates that inertia compensation can counteract the side effects of the exoskeleton inertia on human legs during walking. This motivates us to shape the inertia terms in M_{44}, which only appear in the diagonal of M_{44}. This is equivalent to defining our desired $\tilde{M}_{44}$ by adding an additional diagonal matrix M_D to M_{44}:

$$\begin{aligned}\tilde{M}_{44} &= M_{44} + M_D,\\ M_D &= \text{diag}[(\kappa-1)I_i],\end{aligned}$$

where I_i is the sum of all inertia terms included in $M_{44}(i,i)$, and κ is defined as the inertia scaling factor, i.e., $\tilde{I}_i = \kappa\cdot I_i$ in $\tilde{M}_{44}$. By choosing $\tilde{M}_{44}$ in this fashion, we will have $\tilde{C} = C$ since $\partial M_D/\partial q = 0$. As for potential energy, we choose $\tilde{N} = \mu N$ to provide both positive ($\mu < 1$) and negative ($\mu > 1$) BWS as in [21]. In simulations, we will try different combinations between κ and μ and simulate walking accordingly.

B. Simulation Methods

In order to predict the effects of energy shaping on human locomotion, we must first construct a human-like, stable walking gait in simulation. Following the same convention in [21], we define the human torque for a single joint in v as:

$$\mathrm{v}_j = -K_{\mathrm{p}j}(\theta_j - \theta_j^{\mathrm{eq}}) - K_{\mathrm{d}j}\dot{\theta}_j, \tag{40}$$

where $K_{\mathrm{p}j}$, $K_{\mathrm{d}j}$, θ_j^{eq} respectively correspond to the stiffness, viscosity, and equilibrium angle of joint $j \in \{\mathrm{a},\mathrm{k},\mathrm{h},\mathrm{sk},\mathrm{sa}\}$. We adopted the same values of parameters in our previous paper [21], and these parameters were kept constant in the simulation to isolate the effects of energy shaping.

Biped locomotion is modeled as a hybrid dynamical system which includes continuous and discrete dynamics. For the biped model we used in this paper, impacts happen when the swing heel contacts the ground and when contact constraints change between the heel contact and flat foot conditions. The following sequence that includes hybrid dynamics and impact maps during one step is a review of Section V-B in [21]:

1. $M\ddot{q} + T(q,\dot{q}) + A_{\text{heel}}^T\lambda = \tau$ if $a_{\text{flat}} \neq 0$,
2. $\dot{q}^+ = (I - X(A_{\text{flat}}X)^{-1}A_{\text{flat}})\dot{q}^-$ if $a_{\text{flat}} = 0$,
3. $M\ddot{q} + T(q,\dot{q}) + A_{\text{flat}}^T\lambda = \tau$ if $|c_{\mathrm{p}}(q,\dot{q})| < l_{\mathrm{f}}$,
4. $\dot{q}^+ = \dot{q}^-, (q(1)^+, q(2)^+)^T = \mathcal{G}$ if $|c_{\mathrm{p}}(q,\dot{q})| = l_{\mathrm{f}}$,
5. $M\ddot{q} + T(q,\dot{q}) + A_{\text{toe}}^T\lambda = \tau$ if $h(q) \neq 0$,
6. $(q^+,\dot{q}^+) = \Theta(q^-,\dot{q}^-)$ if $h(q) = 0$,

where $X = M^{-1}A_{\text{flat}}^T$, and $\mathcal{G} = (l_{\mathrm{f}}\cos(\gamma), l_{\mathrm{f}}\sin(\gamma))^T$ models the change in IRF. The vector $c_{\mathrm{p}}(q,\dot{q})$ is the COP defined with respect to the heel IRF calculated using the conservation law of momentum. The vector T groups the Coriolis/centrifugal terms and potential forces for brevity. The ground clearance of the swing heel is denoted by $h(q)$, and Θ denotes the swing heel ground-strike impact map derived based on [25]. Note that the aforementioned sequence of continuous and discrete dynamics repeats after a complete step, i.e., phase 6 switches back to phase 1 for the next step.

Due to the difficulty of analytically proving stability for hybrid systems in general, we checked local stability

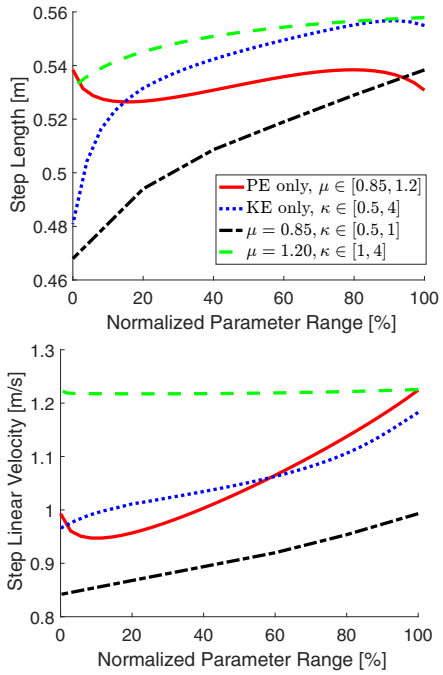

Fig. 3. The step length and step linear velocity with four different shaping strategies during Lyapunov funneling process. The two figures share the same legend and are plotted with normalized x-axes, e.g., $\mu = 0.85$ indicates 0% and $\mu = 1.2$ indicates 100% on the x-axes in the PE curves.

numerically by applying the Poincaré method. Letting $x = (q^T, \dot{q}^T)^T$ be the state vector of the biped, a walking gait corresponds to a periodic solution curve $\bar{x}(t)$ of the hybrid system such that $\bar{x}(t) = \bar{x}(t+T)$, for all $t \geq 0$ and some minimal $T > 0$. The set of states occupied by the periodic solution defines a *periodic orbit* $\mathcal{O} := \{x | x = \bar{x}(t) \text{ for some } t\}$ in the state space. The step-to-step evolution of a solution curve can be modeled with the *Poincaré* map $\mathcal{P} : G \to G$, where $G = \{x | h(q) = 0\}$ is the switching surface indicating initial heel contact [23]. The intersection of a periodic orbit with the switching surface is a fixed point $x^* = \mathcal{P}(x^*)$. We can linearize the Poincaré map about this point to analyze the local stability of the hybrid dynamical system according to the standard result in [26]. If the eigenvalues of the Jacobian $\nabla_{x_e} \mathcal{P}(x_e^*)$ are within the unit circle, where $x_e^* = G \cap \mathcal{O}$, then the periodic orbit $\mathcal{O}$ is locally exponentially stable in the hybrid system. The eigenvalues are calculated in simulation by first allowing the biped to converge to a fixed point and then performing the perturbation analysis described in [14].

C. Results and Discussion

The following simulations utilized the model parameters from [20, Table I]. The mass and inertia of the exoskeleton were neglected to simplify the analysis and find generic properties independent of any particular exoskeleton design. These exoskeleton parameters can be compensated by the energy shaping controller in future experimental implementations. The human input (40) provided a nominal walking gait, from which we observed the effect of potential energy shaping by progressively changing the BWS ratio μ while keeping $\kappa = 1$, i.e., not shaping kinetic energy. Analogously, we fixed $\mu = 1$ while gradually changing κ to study the independent effects of kinetic energy shaping. Finally, we fixed μ to specific numbers (e.g., 0.8 and 1.2) and again progressively changed κ to observe the effects of total energy shaping. Singularities in $\tilde{M}_\lambda$ were avoided during this progressive tuning process, known as Lyapunov funneling [27]. For each choice of parameters κ, μ, the walking gait was allowed to converge to steady-state before recording features of the gait.

TABLE I

EXAMINED COMBINATIONS OF κ AND μ

Combinations	κ	μ
Potential Energy Shaping	1	$[0.85, 1.2]$
Kinetic Energy Shaping	$[0.5, 4]$	1
Total Energy Shaping	$[0.5, 1]$	0.85
Total Energy Shaping	$[1, 4]$	1.2

Due to the sensitivity of the nominal passive gait, we could only decrease/increase κ and μ within the ranges reported in Table I, after which there was insufficient/excessive energy to maintain a stable gait. Because the shapeable ranges of κ and μ differ greatly, the progressive effect on gait parameters are shown over normalized changes in shaping terms κ and μ in Fig. 3. For both potential and kinetic energy shaping, we can see a decrease in step length and step linear velocity when choosing $\kappa < 1$ or $\mu < 1$, whereas an increase can be observed when choosing $\kappa > 1$ or $\mu > 1$ (except for extreme ranges). Given a certain percentage of virtual BWS, total energy shaping controllers achieved higher ($\kappa > 1$, $\mu = 1.2$) and lower ($\kappa < 1$, $\mu = 0.85$) values in both the step length and step linear velocity curves, compared to only shaping the potential energy. This indicates that adding kinetic energy shaping in addition to potential energy shaping can further augment step length and step linear velocity, which could help patients to accelerate/decelerate during walking.

For a joint-level perspective, Fig. 4 compares the phase portraits of the passive gait and two shaped gaits ($\kappa = 4, \mu = 1.2$ vs. $\kappa = 0.5, \mu = 0.85$). The phase portraits contract in both axes when both κ and μ are chosen to be less than 1, i.e., decreasing total energy. This observation aligns with the decrease in step length and linear velocity seen in Fig. 3 as κ and μ decrease. When choosing κ and μ to be greater than 1 (increasing total energy), we instead see an expansion in all phase portraits except for the swing ankle.

CONCLUSION

This paper generalized the constrained framework from previous work [20], [21] and derived an exoskeletal control strategy for augmenting step length and step linear velocity via total energy shaping. The closed-loop energy that can be altered via control was determined by a generalized matching condition defined from Lagrangian dynamics with holonomic contact constraints. Given a certain amount of virtual BWS, kinetic energy shaping can further augment step length and step linear velocity, helping patients to accelerate/decelerate during gait training. Created as a rehabilitation tool, this shaping strategy could potentially reduce physical labor from clinicians and enable training outside the clinic. Future work will explore other possible forms of energy modification and

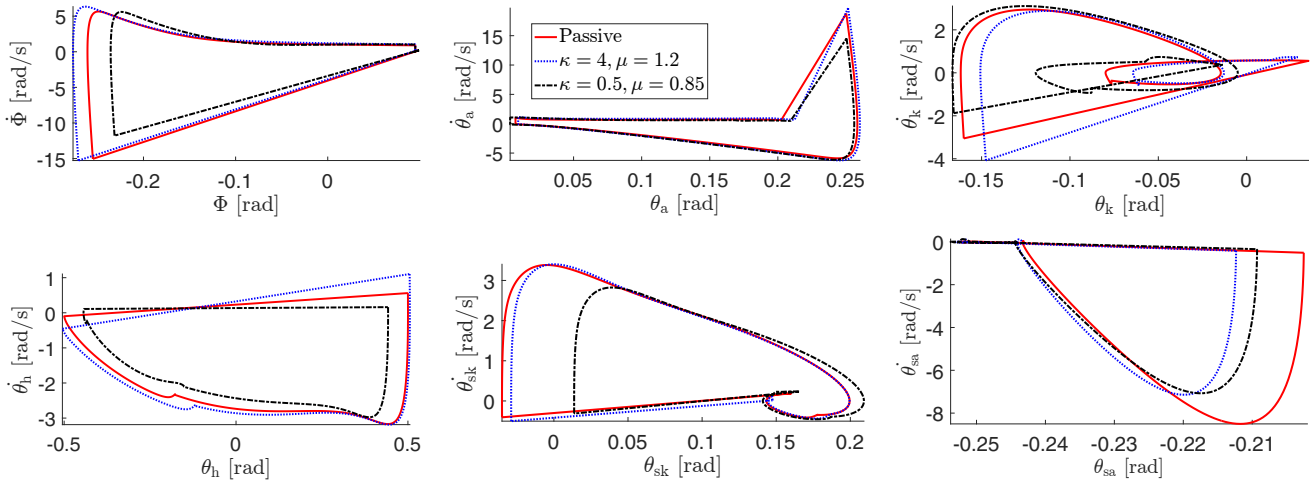

Fig. 4. Phase portraits of ϕ (top left), stance ankle (top center), stance knee (top right), hip (bottom left), swing knee (bottom center), and swing ankle (bottom right) of the passive gait and the controlled gaits ($\kappa = 4, \mu = 1.2$ and $\kappa = 0.5, \mu = 0.85$) during one steady step. All these figures share the same legend.

establish possible passivity properties between the human user and the exoskeleton. Other work will include experimental implementations of this control strategy on powered exoskeletons including [28].

REFERENCES

[1] S. J. Olney, T. N. Monga, and P. A. Costigan, "Mechanical energy of walking of stroke patients," *Arch. Phys. Med. Rehabil.*, vol. 67, no. 2, pp. 92–98, 1986.

[2] H. Vallery, E. H. van Asseldonk, M. Buss, and H. van der Kooij, "Reference trajectory generation for rehabilitation robots: complementary limb motion estimation," *IEEE Trans. Neural Syst. Rehabil. Eng.*, vol. 17, no. 1, pp. 23–30, 2009.

[3] D. Sanz Merodio, M. Cestari Soto, J. C. Arevalo, and E. García Armada, "Control motion approach of a lower limb orthosis to reduce energy consumption," *Int. J. Adv. Robot. Syst.*, vol. 9, pp. 1–8, 2012.

[4] K. Suzuki, G. Mito, H. Kawamoto, Y. Hasegawa, and Y. Sankai, "Intention-based walking support for paraplegia patients with robot suit HAL," *Adv. Rob.*, vol. 21, no. 12, pp. 1441–1469, 2007.

[5] K. A. Strausser and H. Kazerooni, "The development and testing of a human machine interface for a mobile medical exoskeleton," in *2011 IEEE/RSJ Int. Conf. Intell. Robot. Syst.*, 2011, pp. 4911–4916.

[6] H. A. Quintero, R. J. Farris, C. Hartigan, I. Clesson, and M. Goldfarb, "A powered lower limb orthosis for providing legged mobility in paraplegic individuals," *Topics in Spinal Cord Injury Rehabilitation*, vol. 17, no. 1, p. 25, 2011.

[7] T. Yan, M. Cempini, C. M. Oddo, and N. Vitiello, "Review of assistive strategies in powered lower-limb orthoses and exoskeletons," *Rob. Auton. Syst*, vol. 64, pp. 120–136, 2015.

[8] T. G. Hornby, D. H. Zemon, and D. Campbell, "Robotic-assisted, body-weight–supported treadmill training in individuals following motor incomplete spinal cord injury," *Physical therapy*, vol. 85, no. 1, pp. 52–66, 2005.

[9] U. Nagarajan, G. Aguirre-Ollinger, and A. Goswami, "Integral admittance shaping: A unified framework for active exoskeleton control," *Rob. Auton. Syst.*, vol. 75, pp. 310–324, 2016.

[10] J. Ghan, R. Steger, and H. Kazerooni, "Control and system identification for the Berkeley Lower Extremity Exoskeleton (BLEEX)," *Adv. Rob.*, vol. 20, no. 9, pp. 989–1014, 2006.

[11] G. Aguirre-Ollinger, J. E. Colgate, M. A. Peshkin, and A. Goswami, "Inertia compensation control of a one-degree-of-freedom exoskeleton for lower-limb assistance: Initial experiments," *IEEE Trans. Neural Syst. Rehabil. Eng.*, vol. 20, no. 1, pp. 68–77, 2012.

[12] S. A. Murray, K. H. Ha, C. Hartigan, and M. Goldfarb, "An assistive control approach for a lower-limb exoskeleton to facilitate recovery of walking following stroke," *IEEE Trans. Neural Syst. Rehabil. Eng.*, vol. 23, no. 3, pp. 441–449, 2015.

[13] R. D. Gregg and M. W. Spong, "Reduction-based control of three-dimensional bipedal walking robots," *The International Journal of Robotics Research*, vol. 29, no. 6, pp. 680–702, 2010.

[14] R. D. Gregg, Y. Y. Dhaher, A. Degani, and K. M. Lynch, "On the mechanics of functional asymmetry in bipedal walking," *IEEE Trans. Biomed. Eng*, vol. 59, no. 5, pp. 1310–1318, 2012.

[15] M. W. Spong, "The passivity paradigm in bipedal locomotion," in *Proceedings of the International Conference on Climbing and Walking Robots*, Madrid, Spain, 2004.

[16] M. W. Spong and F. Bullo, "Controlled symmetries and passive walking," *IEEE Trans. Autom. Control*, vol. 50, no. 7, pp. 1025–1031, 2005.

[17] J. Holm, "Gait regulation for robotic bipedal locomotion," Ph.D. dissertation, University of Illinois at Urbana-Champaign, 2008.

[18] J. K. Holm and M. W. Spong, "Kinetic energy shaping for gait regulation of underactuated bipeds," *Proc. IEEE Int. Conf. Control Appl.*, pp. 1232–1238, 2008.

[19] R. D. Gregg, A. Tilton, S. Candido, T. Bretl, and M. Spong, "Control and planning of 3-d dynamic walking with asymptotically stable gait primitives," *IEEE Trans. Rob.*, vol. 28, no. 6, pp. 1415–1423, 2012.

[20] G. Lv and R. D. Gregg, "Orthotic body-weight support through underactuated potential energy shaping with contact constraints," in *Proc. IEEE Conf. Decis. Control*, 2015, pp. 1483–1490.

[21] ——, "Underactuated potential energy shaping with contact constraints: Application to a powered knee-ankle orthosis," *IEEE Trans. Control Syst. Technol.*, 2017.

[22] G. Lv, H. Zhu, T. Elery, L. Li, and R. D. Gregg, "Experimental implementation of underactuated potential energy shaping on a powered ankle-foot orthosis," in *IEEE Int. Conf. Robot. Autom.*, 2016, pp. 3493–3500.

[23] R. D. Gregg, T. Lenzi, L. J. Hargrove, and J. W. Sensinger, "Virtual constraint control of a powered prosthetic leg: From simulation to experiments with transfemoral amputees," *IEEE Trans. Rob.*, vol. 30, no. 6, pp. 1455–1471, Dec. 2014.

[24] G. Blankenstein, R. Ortega, and A. J. Van Der Schaft, "The matching conditions of controlled lagrangians and ida-passivity based control," *Int. J. Control*, vol. 75, no. 9, pp. 645–665, 2002.

[25] E. R. Westervelt, J. W. Grizzle, and D. E. Koditschek, "Hybrid zero dynamics of planar biped walkers," *IEEE Trans. Autom. Control*, vol. 48, no. 1, pp. 42–56, 2003.

[26] J. Grizzle, E. Westervelt, C. Chevallereau, J. Choi, and B. Morris, *Feedback Control of Dynamic Bipedal Robot Locomotion*. Boca Raton, FL: CRC Press, 2007.

[27] R. D. Gregg, "Geometric control and motion planning for three-dimensional bipedal locomotion," Ph.D. dissertation, University of Illinois at Urbana-Champaign, 2010.

[28] H. Zhu, J. Doan, C. Stence, G. Lv, T. Elery, and R. D. Gregg, "Design and validation of a torque dense, highly backdrivable powered knee-ankle orthosis," *IEEE Int. Conf. Robot. Autom.*, 2017.